Powering Earth's ancient dynamo with silicon precipitation

Alfred J. Wilson
School of Earth and Environment, University of Leeds
a.j.wilson1@leeds.ac.uk

Monica Pozzo
Department of Earth Sciences, University College London London Centre for Nanotechnology, Thomas Young Centre, University College London
m.pozzo@ucl.ac.uk

Dario Alfé Department of Earth Sciences, University College London London Centre for Nanotechnology, Thomas Young Centre, University College London Dipartimento di Fisica "Ettore Pancini", Universita' di Napoli
d.alfe@ucl.ac.uk

Andrew M. Walker
Department of Earth Sciences, University of Oxford
andrew.walker@earth.ox.ac.uk

Sam Greenwood
School of Earth and Environment, University of Leeds
S.Greenwood@leeds.ac.uk

Anne Pommier
Earth & Planets Laboratory, Carnegie Institution for Science
apommier@carnegiescience.edu Christopher J. Davies School of Earth and Environment, University of Leeds
c.davies@leeds.ac.uk

This is a non-peer reviewed, pre-print manuscript submitted to EarthArXiv, also submitted to Nature Communications.

Powering Earth's ancient dynamo with silicon precipitation

Alfred J Wilson[1*], Monica Pozzo[2,3], Dario Alfè[2,3,4], Andrew M. Walker[5], Sam Greenwood[1], Anne Pommier[6] and Christopher J. Davies[1]

[1*]School of Earth and Environment, University of Leeds, Woodhouse, Leeds, LS2 9JT, UK.
[2]Department of Earth Sciences, University College London, 5 Gower Place, London, WC1E 6BS, UK.
[3]London Centre for Nanotechnology, Thomas Young Centre, University College London, 17-19 Gordon Street, London, WC1H 0AH, UK.
[4]Dipartimento di Fisica "Ettore Pancini", Universita' di Napoli "Federico II", Monte S. Angelo, Napoli, 80126, Italy.
[5]Department of Earth Sciences, University of Oxford, S Parks Rd, Oxford, OX1 3AN, UK.
[6]Earth & Planets Laboratory, Carnegie Institution for Science, 5241 Broad Branch Road, Washington DC, 20015, USA.

*Corresponding author(s). E-mail(s): a.j.wilson1@leeds.ac.uk;

Abstract

Earth's core has produced a global magnetic field for the last 4 Gyrs, presently sustained by inner core growth. Models of the core with high thermal conductivity suggest potentially insufficient power available for the geodynamo prior to inner core formation ∼1 Ga. Precipitation of SiO_2 from the liquid core might offer an alternative power source for the magnetic field before inner core growth, however, no estimates of partition coefficient exist for conditions of the early core. We present the first determination of the silicon partition coefficient at core-mantle boundary conditions and use these results to build a thermodynamic model that

is integrated into a model of coupled core-mantle thermal evolution. We show that models including precipitation of silicon can satisfy constraints of inner core size, mantle convective heat flux, mantle temperature and a persistent ancient geodynamo whilst those excluding fail. Successful power from precipitation favours an oxygen poor initial core composition.

Keywords: Earth's core, geodynamo, thermal evolution, ab initio

1 Introduction

Earth's magnetic field is fundamental for the habitability of our planet, and yet the power to sustain it remains enigmatic for the majority of geological time. Palaeointensity data suggest the field has been maintained for at least the last 3.45 Gyrs [1] but the main power sources derive from growth of the solid inner core [2–4]. Growth of the inner core provides latent heat, however more influential is that light elements can be partitioned into the liquid [5] creating a chemical buoyancy source at the base of the outer core. Oxygen is considered a likely candidate because it can help to explain the density contrast between the inner and outer cores [6] although similar partitioning and convective influence can be explained by carbon [7]. Enrichment of the lowermost outer core in light elements provides power for outer core convection which is expected to be the major contributor to geodynamo power today [2, 8, 9].

Several first principles calculations and high pressure (P) and temperature (T) experimental results suggest that the core thermal conductivity may be significantly higher than previously thought [10–15]. Maintaining sufficient power for the dynamo with high conductivity implies rapid cooling and constrains the inner core to be far less than 1 Gyrs old. It also requires the geodynamo to be powered by heat loss from the core for most of Earth's history. This rapid cooling scenario means the mantle would have been subject to a super-solidus core-mantle boundary (CMB) temperature for much of Earth history [2, 4, 16].

The presence of a basal magma ocean (BMO) may provide a resolution to the ancient geodynamo [17], although this approach relies upon the uncertain evolution of the BMO as well as requiring a conductivity at the lower limit of the recent high estimates. Secular cooling is not an efficient mechanism for powering the geodynamo, making thermal convection alone an unsuitable power source [18].

In search of an alternate explanation for the long-lived geodynamo, prior studies have investigated whether light elements in the liquid core, incorporated during a hot differentiation, might become insoluble during cooling and precipitate. Convection is driven by the dense, iron-rich residual liquids sinking following precipitation. Lower initial core temperatures and slower cooling allowed by this power source imply a significantly older inner core. MgO precipitation has been suggested [18–20] although the dependence of magnesium solubility on the oxygen content of the core has been argued to reduce the overall power output, making MgO precipitation an insufficient power source for the geodynamo alone [21, 22]. Additionally, incorporating sufficient Mg in the core initially is difficult due to limited solubility in iron liquids. Others have investigated the possibility of precipitating Si [23, 24] which is a more widely accepted component in the liquid core (e.g. 25–27) as well as simultaneous precipitation of multiple elements [28]. At present, there is no consensus on the possibility of Si precipitation, nor its onset time or associated power. This is due to uncertainties on the initial composition of the core [26, 29, 30], the method of modelling the partitioning behaviour, and the lack of data at core conditions. Here we will address all three of these.

We produce the first determinations of Si partitioning at CMB conditions. Ab initio molecular dynamic simulations of iron-rich liquids and silicate liquids are used to calculate chemical potentials through free energy differences.

Equilibrium constants calculated from these chemical potentials are in good agreement with the extrapolation of previous experimental results at lower pressures and temperatures than core pressure. We derive a thermodynamic model for Si partitioning using a dataset which spans a wider range of physical and chemical conditions than was available to previous studies and confirm the extrapolation of this model to core conditions with our ab initio results. We use our thermodynamic model to describe Si precipitation in thermal history models of the cooling core. Previous studies of SiO_2 have evaluated the cooling rate needed to sustain a geodynamo from experimentally derived precipitation rates [23] and implemented a thermodynamic model of simultaneous precipitation of multiple light elements into a parameterised model of core thermal evolution [28]. We take a combined approach, using a thermal evolution model whilst choosing to focus solely on Si precipitation with a greater number of resolved interaction parameters. This includes C, O, Si, S, Mg in order to capture important compositional effects relevant to all commonly considered light elements in the core. Si precipitation is considered over SiO_2 to isolate its effect on the thermal evolution of the core and avoid uncertainty associated with the type and source of reactants.

2 Results and Discussion

2.1 Ab initio calculations

Si distribution coefficients (K_d) are calculated for the first time at early core conditions using excess chemical potentials; the difference in chemical potentials of a species on either side of a reaction ($\delta\tilde{\mu}_{SiO_2} = \tilde{\mu}^{metal}_{SiO_2} - \tilde{\mu}^{silicate}_{SiO_2}$). Chemical potentials are calculated through free energies differences at represent significant computational expense. For a dissociation reaction

($K_d^{dissociation} = \frac{x_{Si}^{metal} x_O^{metal\,2}}{x_{SiO_2}^{silicate}}$, other reactions computational details are discussed in methods and supplementary information) $K_d = 0.50^{-0.09}_{+0.1}$ at 5500 K and $0.029^{-0.014}_{+0.028}$ at 4500 K, both at 124 GPa. Differences in compositions make direct comparison difficult but indicate an overall agreement in trends. The highest PT experiments compare well to our results especially at 4500 K, which lies within the scatter of experiments at similar temperatures. This dataset shows a strong temperature dependence and a weaker pressure effect, especially above 50 GPa, commensurate with an entropy dominated, configurational change in the iron-rich liquid and in agreement with other high PT partitioning studies (e.g. 20, 27).

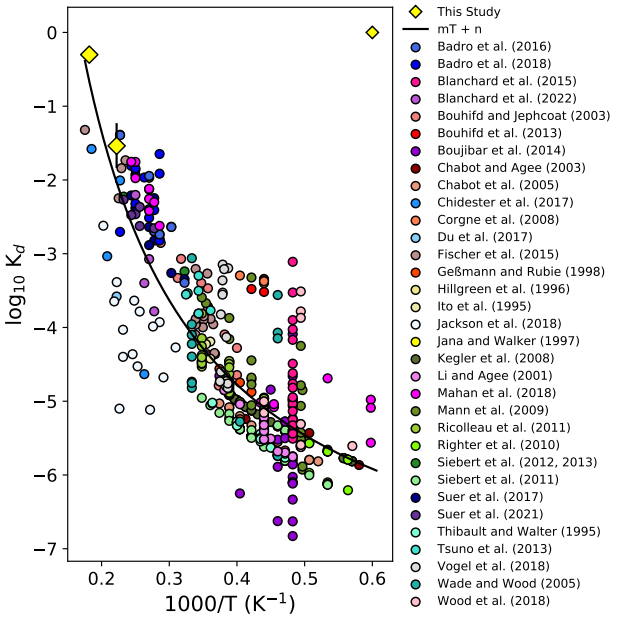

Fig. 1 Comparison of partition coefficients for the dissociation of Si and O into Fe-rich liquid calculated from our experimental dataset using our thermodynamic model with ab initio results of this study (yellow diamonds). The complete dataset is presented in the supplementary information (table S1). We show a fit of these values of K_d to a general temperature dependence (black line, $\log_{10} K_d = mT + n$ where m = 609.5 and n = 218.4).

2.2 Thermodynamic Model

To evaluate Si solubility in the liquid core, we must know the T, P and compositional influences on partitioning. Ab initio results provide T dependence of K_d naturally, however, a thermodynamic model is required for compositional effects. We construct a thermodynamic model of partitioning fit to lower P and T experimental data and validate extrapolation using our ab initio results. We use an interaction parameter model [31] which is commonly applied to high PT partitioning reactions (e.g. 20, 23, 27, 32). The interaction parameters are notionally universal and constant, however in reality, data are insufficient to fully resolve all possible parameters. This is because the existing data do not fully span P, T and composition space for the core. Varying starting compositions among studies also limits the interactions which can be resolved and affects partitioning behaviour, given that omission of one element can affect the interactions between retained elements. Additionally, differing experimental techniques introduce various uncertainties making any direct comparison challenging. Finally, the interaction parameter model is designed for solutes at low concentration, many studies include elements of interest in high concentration in order to better resolve their effects, but these may not be fully captured by this type of model. It is therefore inevitable that the interaction parameters will vary based on these factors. Indeed this is made apparent by previous studies [20, 27, 32] as well as in this study. To circumvent these difficulties, we have gathered the largest dataset yet (see supplementary information) in order to best constrain Si partitioning behaviour. Our model uses values which provide the best fit to our dataset. However, fixing specific parameters to the values found by previous studies can still produce models which predict precipitation rates within the error of our model.

We find that the aggregate temperature dependence of K_d from our model is 0.0014 K^{-1} on average, which is within the uncertainty of our ab initio results (0.0016 - 0.00086 K^{-1}). The dominant compositional effect is that O limits the solubility of Si in agreement prior studies [23]. Fig. 2 shows the prediction of stable Si concentration and precipitation from our thermodynamic model. For moderate O concentrations (0.4-1 wt. %) and temperatures between 3500 and 6000 K, we find precipitation rate in the range of 2×10^{-3} to 3×10^{-4} wt.% K^{-1}. The precipitation rates predicted by functional models incorporating interaction parameters from previous studies occupies a range narrower than that imposed by the uncertainty of the initial O content of the core (fig. 2). One notable prediction of our model is that the range of initial Si concentrations predicted by accretionary modelling will encompass the compositions found to be consistent with inner core density jumps of 0.8 and 1.0 g cm^{-1}, whilst excluding higher contrasts. Considering more complex compositions will influence the absolute solubility of Si, although, significantly higher concentrations are unlikely due to the dominant effect of temperature and O content.

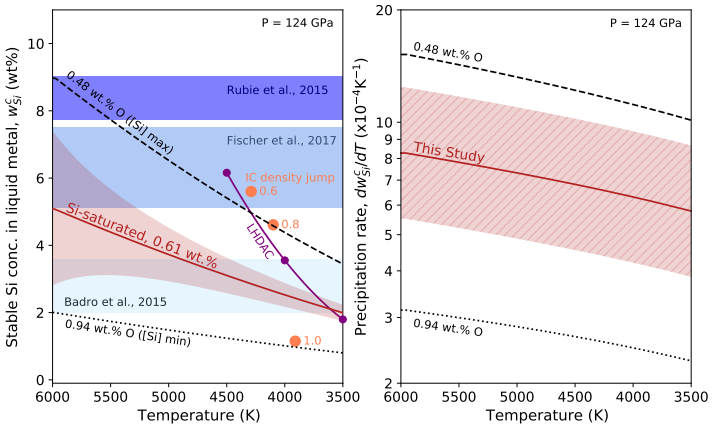

Fig. 2 Left: Stable concentration of Si in the liquid metal. Our model is evaluated for partitioning between an initially Si saturated iron-rich liquid containing 0.61 wt. % O and a pyrolite mantle (red solid line) at 124 GPa. Red shaded envelope is the uncertainty from the fitting parameters of our model. Horizontal shaded regions are estimated initial high [26] (dark blue), moderate [30] (mid blue) and low [29] (light blue) core Si content. Orange circles are estimates of present-day core composition [33] (within an Fe-Si/S-O core) based on the inner core density jump of 0.6, 0.8 and 1.0 g cm^{-3}. Laser heated diamond anvil cell experiments [23] are shown as purple circles. Dotted (dashed) line is the minimum (maximum) initial Si concentration [26, 29] with initial O concentration set to achieve this. Right: Precipitation rate from our model, hatched shaded region of 1.5x and 0.67x encompasses functional models using parameters fixed to values found from previous studies. Maximum and minimum initial Si cases are also shown

2.3 Thermal evolution of the core

To investigate the effect of precipitation on the thermal evolution of the core we combine two classical models of the core [17, 34] and the solid mantle [35]. These parameterisations of the deep Earth are coupled at the CMB, where the mantle defines the heat transport across the CMB and the core defines the temperature of the CMB. For the core, energy balance is used to evolve the core temperature and composition alongside entropy balance to evaluate the entropy production due to the magnetic field. A moderately high conductivity

scenario is considered, where thermal conductivity is 70 W m^{-1} K^{-1} everywhere in the core [15, 17]. Whilst a solid mantle is included, we do not include a separate magma ocean to minimise the contributions to geodynamo power such that the effects of precipitation are clearly distinguishable and the number of uncertain parameters is reduced. This setup is not fully consistent with our thermodynamic model, which is based on liquid-liquid reactions in both experiments and calculations, but is preferable to attempting to model the highly uncertain physics associated with a magma ocean. Due to the high CMB temperatures present in many of our models, we envisage (purely for convenience) a simplistic, persistent thin melt layer at the base of the mantle, with negligible latent heat release and an equal partitioning of radiogenic elements (which we do not expect to be the case in reality) with the overlying mantle. We assume that the core is mixed thoroughly on timescales far shorter than the timestep of our simulation such that the liquid core has no compositional variation nor chemically stable layers. We do observe sub adiabatic CMB heat flux prior to inner core nucleation in our models implying thermally stratified layers at the top of the liquid core.

Our description of precipitation is based solely on the thermodynamic stability of Si, depending on P, T and composition. We evaluate precipitation as removing the fraction of Si above the stability limit from the metal and do not include oxygen in this evaluation. This is done to pose the simplest case when examining the power made available to the geodyanmo and also to avoid the need to include a description of phase (e.g. SiO_2 or SiC) or source of reactant (e.g. mantle, core or boundary layer) both of which are highly uncertain.

The thermal history of two compositional scenarios is considered; high (10 mol%) and low (2 mol%) initial oxygen compositions of the liquid core, all with a pyrolitic mantle composition. Table 1 provides the setup parameters for each

case. The mantle composition is held constant for a simple examination of the effect of core evolution. We expect that the mantle composition would not be greatly affected by precipitation because it is a significantly larger reservoir of Si than the core, however the effect of a freezing basal magma ocean may be more significant. Each initial core composition is evolved under conditions of initially over- and under-saturated Si content, and with ($\alpha^i_{ppt} \neq 0$) and without ($\alpha^i_{ppt} = 0$) the convective power of precipitation included. We vary the upper to lower mantle viscosity ratio (f_{visco}) and initial CMB temperature ($T^{cmb}_{t=0}$) to regulate the core temperature such that the final state of our models matches constraints of the present-day core. These constraints are: the inner core radius agreeing with the present-day value of 1221 km, a present-day mantle convective heat flow of 39 TW [36], a mid-mantle temperature of 2320 K, and a positive entropy from ohmic dissipation (or dynamo entropy, E_j) for all time preceding inner core nucleation.

	Symbol	O	Si	α^O_{ppt}	α^{Si}_{ppt}	$T^{CMB}_{t=0}$	f_{visco}
	Units	wt. %	wt. %			K	
Without Precipitation	A	5.314	0.165	0.0	0.0	5500	4
	B	5.303	0.085	0.0	0.0	5200	5
	C	1.126	4.339	0.0	0.0	7000	23
	D	1.070	2.137	0.0	0.0	6500	12
With Precipitation	A^P	5.314	0.165	1.1	0.87	5000	5
	B^P	5.303	0.085	1.1	0.87	4900	6
	C^P	1.126	4.339	1.1	0.87	5400	13
	D^P	1.070	2.137	1.1	0.87	5800	9

Table 1 Initial values for thermal evolution model runs (A-D^P) where all other quantities remain unchanged from the original models of core [4] and mantle [35] unless otherwise stated. Expansivity (α^i_{ppt}) [33] applies only to precipitation from the liquid core, non-zero values are applied to inner core growth for all cases. High (A,A^P,B,B^P) and low (C,C^P,D,D^P) oxygen cases are taken for Si over (A,A^P,C,C^P) and under (B,B^P,D,D^P) saturation with power from precipitation turned on (A^P-D^P) and off (A-D). Parameters $T^{CMB}_{t=0}$ and f_{visco} (ratio of upper to lower mantle viscosity) are varied to match present day constraints.

Fig. 3 shows examples of the time evolution of inner core radius, mid-mantle potential temperature, CMB temperature, mantle convective heat flow, CMB heat flow, and dynamo entropy for two cases that differ by the inclusion or emission of precipitation. We find that without precipitation all cases will fail to maintain a positive dynamo entropy before inner core nucleation. This is because secular cooling must be sufficiently diminished by rapid cooling to grow the inner core to the present day size. We find that including the energy and entropy effects of precipitation can maintain a positive E_j for the majority of Earth history preceding inner core formation, producing an older inner core. We find that high initial oxygen concentration cases strongly reduce available dissolved silicon and therefore power from precipitation. These cases require $f_{visco} < 7$ in order to grow the core to present-day size, meaning the mantle is responsible for maintaining rapid secular cooling. This highlights the requirement for modest O content for Si precipitation to reduce mantle and core temperatures, sustain a geodynamo and satisfy present-day constraints. We find that compared to cases without precipitation, continuous precipitation of Si from the liquid core can sustain the geodynamo throughout Earth's history and allow the core to be 300 K cooler and 500 Myrs older.

We also examine the effect of doubling and halving the calculated precipitation rate to explore the uncertainty of our thermodynamic model (shaded region, fig. 2). Although this requires minor adjustment of initial T^{CMB} and f_{visco}, the same outcome of cases with precipitation meeting all four constraints is held whilst inner core ages differ by <100 Myrs and ancient core temperatures by $<$ 50 K. This shows that different combinations of interaction parameters in the thermodynamic model can produce some variance in the calculated precipitation rate, but this is not large enough to change the outcome of the thermal evolution. We also show that the uncertainty on the

initial oxygen content (dashed and dotted lines, fig 2) of the core has a far greater effect on the outcome of thermal evolution models than the uncertainty of thermodynamic modelling.

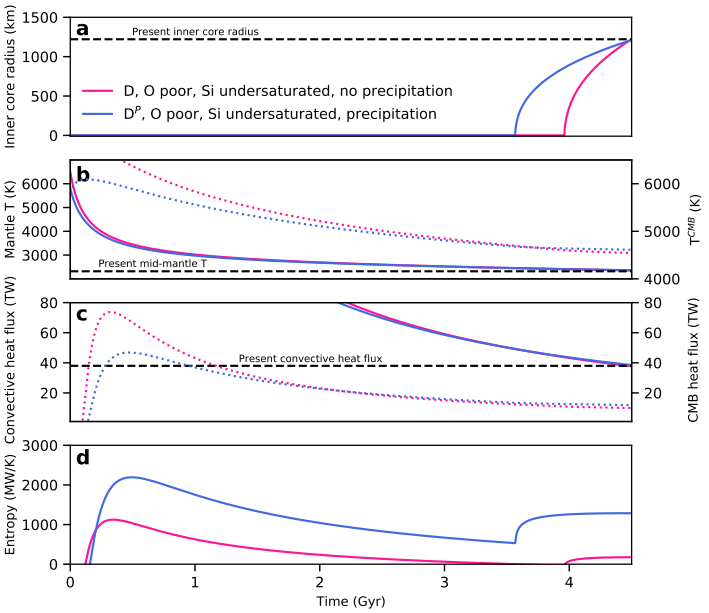

Fig. 3 Thermal evolution of the Earth's core with an initial condition of low O concentration (2 mol%) and Si saturation with inclusion (blue) and exclusion (pink) of power and entropy of precipitation (cases C and C$^{\mathrm{P}}$ from Table 1, respectively). Inner core radius (a), mid-mantle potential temperature (b, left, solid lines) and CMB temperature (b, right, dotted lines), convective mantle heat flux (c, left, solid lines) and CMB heat flow (c, right, dotted), and core entropy from ohmic dissipation (d). Black dashed lines show present-day target values.

We show the outcomes of thermal history cases from table 1 in fig. 4. When Si is initially saturated (cases A, A$^{\mathrm{P}}$ and C, C$^{\mathrm{P}}$) the low O cases require high values of f_{visco} for the inner core to not grow too large by 4.5 Gyrs whilst in the high O case low temperatures are needed to freeze the inner core due to further melting point depression. When $Q_{ppt} \neq 0$ (again for Si saturated

initial conditions, cases A^P and C^P) cooling rates are lower and the inner core is ∼500 Myrs older for O poor conditions (more Si is available to precipitate). For cases of initial Si undersaturation (B, B^P, D, D^P; meaning precipitation is delayed by between 130 and 210 Myrs when $\alpha \neq 0$), a similar core temperature is needed both with and without precipitation, however, in all compositional configurations the inner core is older with the precipitation power included [23]. When Si is initially saturated, including Q_p allows lower cooling rates and an older inner core (C^P = 1102 Myrs). Whilst all considered cases are able to produce a geodynamo within the first 2 Gyrs, cases where $Q_{ppt} = 0$ are unable to produce a magnetic field from at least 200 Myrs prior to inner core formation (crossed symbols, fig. 4).

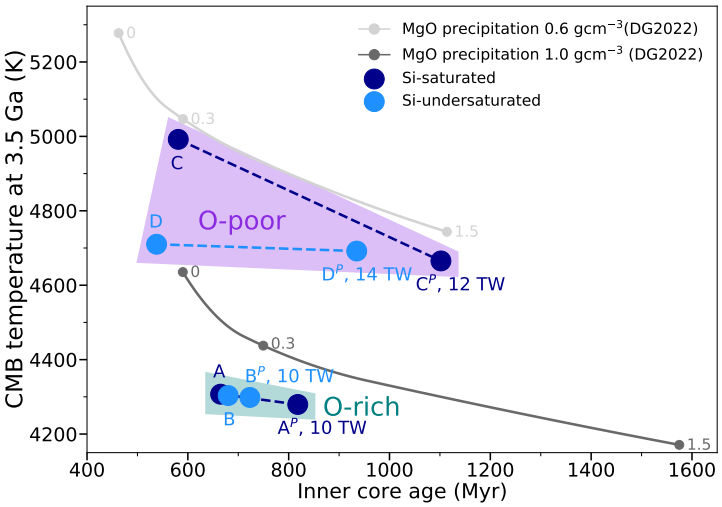

Fig. 4 Inner core age and core temperature at 3.5 Ga for our model with and without convective power from precipitation (connected by dashed lines). Initial Si saturation (undersaturation) is shown as dark (light) blue. O rich (poor) initial conditions are captured by teal (purple) regions. Labels correspond to setup conditions in table 1 and also give the CMB heat flow at 3.5 Ga for models which maintain positive E_j for all time. Also shown are the results from models examining MgO precipitation [17] for precipitation rates of 0, 0.3 and 1.5 $\times 10^{-5}$ K^{-1}, colours denote the core properties in terms of the density jump at the inner core boundary (0.6 (light grey) and 1.0 g cm^{-3} (dark grey)) which represent bounding extremes of the density jump.

We find that the precipitation of Si allows the early core to cool more slowly than it would otherwise and can supply power to the geodynamo throughout Earth's history. High O concentration in the core can reduce ancient core temperatures but relies predominantly on secular cooling to power the ancient geodynamo. The more plausible low O cases result in higher ancient CMB temperatures due to lesser melting point depression. The rheological transition of the magma ocean should occur between 40% to 60% melt fraction [37, 38], rather than at the intersection of the liquidus or solidus, which would correspond to the occurrence of complete crystallisation and first partial melt,

respectively. Our thermal histories for low O content in particular suggest a long lived basal magma ocean. A scenario where the ancient geodynamo is powered by Si precipitation places constraint on accretionary models of core composition. We show that an initial core composition of 4.3 wt. % Si and 1.1 wt. % O is both thermodynamically stable and able to produce sufficient power for the ancient geodynamo to be sustained, however this limits compatible accretion models to those which predict intermediate initial core Si content and low O content.

3 Methods

3.1 Ab Initio Calculations

We conduct density functional theory [39, 40] spin-polarised, molecular dynamic simulations of silicate and iron-rich liquids to calculate the excess chemical potentials of individual chemical components. These calculations individually require significant computational resources, the two partitioning results we present represent millions of CPU hours spread across several HPC systems. Chemical potentials (μ_i) can be described as the free-energy change (∂F) of a system when the quantity of a species (i) is changed

$$\mu_i \left(v, T, x_i, x_j, ...\right) = \left(\frac{\partial F}{\partial x_i}\right)_{V,T,x_i,x_j,..}, \tag{1}$$

in this case under conditions of constant volume (V, v is volume per atom), temperature (T) and composition (where x_i is the molar fraction of species i). Helmholtz free energy (F) is used for consistency with the constant volume conditions of our simulations. We use two complementary methods [41] to calculate μ_i. The first method compares F of a reference system against another

with a different number of solute atoms (dN_i) to isolate μ_i of the solute:

$$\mu_i(v, T, x_i, x_j ...) = \frac{F(V, T, x_i, x_j, ...) - F(V, T, x_i - dN_i, x_j, ...)}{dN}. \quad (2)$$

The second method computes the change in free energy as a result of changing the number of solute atoms in the same system and calculating the change in free energy. The difference here is that the explicit free energies of two systems are not needed, only the change in free energy (for complete details, see 41). Values from both methods are combined for use here, where their variance gives an uncertainty. We find distribution coefficients (K_d) from our ab initio results of μ_i. When μ_i on either side of a reaction are equal, this component is in thermodynamic equilibrium and each concentration will be stable

$$\mu^{silicate}_{SiO_2}(V, T, x^{silicate}_{SiO_2}, x^{silicate}_j, ...) = \mu^{metal}_{SiO_2}(V, T, x^{metal}_{SiO_2}, x^{metal}_j, ...). \quad (3)$$

Here μ_i is dependent on V, T and composition. Separating out the configurational portion of μ_i gives

$$\begin{aligned} &2\left(k_B T \ln x^{silicate}_O + \tilde{\mu}^{silicate}_O\right) + k_B T \ln x^{silicate}_{Si} \\ &= 2\left(k_B T \ln x^{metal}_O + \tilde{\mu}^{metal}_O\right) + k_B T \ln x_S i^{metal} \end{aligned} \quad (4)$$

whilst $\tilde{\mu}_{SiO_2} = \tilde{\mu}_{Si} + 2\tilde{\mu}_O$ in the liquid, which when rearranged becomes equal to the dissociation distribution coefficient

$$K^{dissociation}_d = \frac{x^{metal}_{Si} {x^{metal}_O}^2}{x^{silicate}_{SiO_2}} = \exp\left(-\frac{\tilde{\mu}^{metal}_{SiO_2} - \tilde{\mu}^{silicate}_{SiO_2}}{k_B T}\right) \quad (5)$$

allowing us to validate our thermodynamic model through comparison of model prediction, experimental value and ab initio calculation. The dissolution and exchange reactions take the forms

$$K_d^{dissolution} = \frac{x_{SiO_2}^{metal}}{x_{SiO_2}^{silicate}} = (x_O^{silicate})^2 \exp - \left(\frac{(\tilde{\mu}_{SiO_2}^{metal} - \tilde{\mu}_{SiO_2}^{silicate})}{k_B T} \right) \quad (6)$$

and

$$\begin{aligned} K_d^{exchange} &= \sum_{i=1}^{N-1} \frac{(x_{FeO}^{silicate})^2}{(x_{Fe}^{metal})^2} \frac{x_{Si}^{metal}}{x_{SiO_2}^{silicate}} \\ &= \left(\frac{x_O^{silicate}}{x_O^{metal}} \right)^2 \left(\frac{x_{Fe}^{silicate}}{x_{Fe}^{metal}} \right)^2 \exp - \left(\frac{(\tilde{\mu}_{SiO_2}^{metal} - \tilde{\mu}_{SiO_2}^{silicate})}{k_B T} \right) \end{aligned} \quad (7)$$

respectively.

We focus on pressure and temperatures relevant to the CMB (124 GPa and 4500-5500 K), as these are the most crucial for the evolution of the core. Simulations were performed using the VASP code [42] in the canonical ensemble using a Nosé thermostat [43] and with the Brillioun Zone sampled at the Γ point. A timestep of 1 fs was used and runs lasted between 10 and 100 ps. The plane wave cutoff was set to 500 eV and the projector augmented wave method [44] was used with the generalised gradient approximation functional PW91 [45]. The number of valence electrons and core radii for Fe, Si and O were 14, 4 and 6, and 1.16, 0.7 and 0.08 Angstroms, respectively. Simulations contained between 148 and 160 atoms, depending on composition (reported in supplementary information).

3.2 Thermodynamic Model

We use an interaction parameter model [31] to describe the solubility of Si in iron-rich liquids. We fit this thermodynamic model to experimental values of

K_d (calculated using eq. 5) through eq. S15 in the supplementary information. The parameters of this model capture the compositional effects of C, O, Si, S and Mg (chosen to represent likely light elements in the core and to account for common impurities in our experimental dataset) as well as pressure and temperature effects. We fit to a larger dataset than was available to previous studies (480 measurements from 33 studies) the details of which, choice of reaction and model parameters are provided in the supplementary information.

3.3 Thermal Evolution model

Thermal evolution modelling follows 4 where, if small terms are ignored, the heat flow across the CMB (Q^{cmb}) is found through the balance of energies

$$Q^{cmb} = Q_s + Q_L + Q_{ppt} + Q_g. \tag{8}$$

Q_s is the secular heat stored in the core and Q_L is the latent heat release due to inner core growth. Q_{ppt} is the gravitational energy from mixing the dense, iron-rich residual liquids post precipitation across the outer core [18]

$$Q_{ppt} = \int_{\infty} \psi \rho \alpha^i_{ppt} \left[C_{ppt} \left(\frac{dT_{cmb}}{dt} \right) \right] dV_c \tag{9}$$

where ρ is density, α^i_{ppt} is expansivity, ψ is gravitational potential, C_{ppt} is the precipitation rate of Si ($C_{ppt} = dw^c_{Si}/dT$ is evaluated through our thermodynamic model), t is time and V_c is volume of the liquid core. Q_g is the gravitational power generated from the preferential partitioning of O into the lowermost liquid core upon freezing. We assume Si to partition evenly between the solid and liquid core [6] such that the growth of the inner core has no direct effect on the Si concentration of the liquid core. The entropy budget of

the core can be balanced [9] by

$$E_j + E_\alpha + E_k = E_s + E_L + E_{ppt} + E_g \tag{10}$$

where E_α is the entropy due to barodiffusion throughout the core which is negligible [4, 9] and so is ignored. E_k is the entropy from thermal conduction and the other terms follow the same notation as their energy counterparts. E_j is the entropy due to ohmic dissipation, used to evaluate whether a geodynamo can be sustained (when positive) and is the output of this balance.

4 Supplementary information

The dataset used in this study is available to download from the supplementary information where details of the ab initio calculations and thermodynamic model are also provided.

5 Acknowledgements

We acknowledge the Natural Environment Research Council (NERC) Grant No. NE/T000228/1, which supports A.J.W., C.D., M.P., D.A and A.M.W.. M.P. and D.A. also receive support from NERC Grant No. NE/R000425/1. and S.G., A.P. and C.D. are supported by NSFGEO-NERC grant No. 1832462 (NSF) NE/T003855/1 (NERC).

Calculations were performed on the Monsoon2 system, a collaborative facility supplied under the Joint Weather and Climate Research Programme, a strategic partnership between the UK Met Office and NERC as well as on the U.K. national service Archer and the successing Archer2 service.

6 Author Contributions

M.P. and D.A. conducted the ab initio portion of this project, producing chemical potentials. A.P. and A.J.W constructed the experimental database and S.G. developed the thermal evolution model codes. This project was the inception of C.D. who provided guidance alongside A.M.W.. A.J.W. analysed the experimental data, constructed the thermodynamic model, conducted thermal evolution simulations and analysis, and was primarily responsible for the writing of this manuscript, to which all authors contributed.

References

[1] Tarduno, J.A., Cottrell, R.D., Watkeys, M.K., Hofmann, A., Doubrovine, P.V., Mamajek, E.E., Liu, D., Sibeck, D.G., Neukirch, L.P., Usui, Y.: Geodynamo, solar wind, and magnetopause 3.4 to 3.45 billion years ago. science **327**(5970), 1238–1240 (2010)

[2] Labrosse, S.: Thermal evolution of the core with a high thermal conductivity. Physics of the Earth and Planetary Interiors **247**, 36–55 (2015)

[3] Nimmo, F.: Energetics of the core. In: Schubert, G. (ed.) Treatise on Geophysics 2nd Edn vol. 8, pp. 27–55. Elsevier, Amsterdam (2015)

[4] Davies, C.J.: Cooling history of Earth's core with high thermal conductivity. Physics of the Earth and Planetary Interiors **247**, 65–79 (2015)

[5] Braginsky, S.: Structure of the f layer and reasons for convection in the earth's core. In: Soviet Phys. Dokl., vol. 149, pp. 8–10 (1963)

[6] Alfè, D., Gillan, M., Price, G.D.: Composition and temperature of the Earth's core constrained by combining ab initio calculations and seismic data. Earth and Planetary Science Letters **195**(1-2), 91–98 (2002)

[7] Li, Y., Vočadlo, L., Alfè, D., Brodholt, J.: Carbon partitioning between the Earth's inner and outer core. Journal of Geophysical Research: Solid Earth **124**(12), 12812–12824 (2019)

[8] Buffett, B.A., Huppert, H.E., Lister, J.R., Woods, A.W.: On the thermal evolution of the Earth's core. Journal of Geophysical Research: Solid Earth **101**(B4), 7989–8006 (1996)

[9] Gubbins, D., Alfe, D., Masters, G., Price, G.D., Gillan, M.: Gross thermodynamics of two-component core convection. Geophysical Journal International **157**(3), 1407–1414 (2004)

[10] Pozzo, M., Davies, C., Gubbins, D., Alfè, D.: Thermal and electrical conductivity of iron at Earth's core conditions. Nature **485**(7398), 355–358 (2012)

[11] de Koker, N., Steinle-Neumann, G., Vlček, V.: Electrical resistivity and thermal conductivity of liquid Fe alloys at high P and T, and heat flux in Earth's core. Proceedings of the National Academy of Sciences **109**(11), 4070–4073 (2012)

[12] Gomi, H., Ohta, K., Hirose, K., Labrosse, S., Caracas, R., Verstraete, M.J., Hernlund, J.W.: The high conductivity of iron and thermal evolution of the Earth's core. Physics of the Earth and Planetary Interiors **224**, 88–103 (2013)

[13] Zhang, Y., Hou, M., Liu, G., Zhang, C., Prakapenka, V.B., Greenberg, E.,

406 Fei, Y., Cohen, R., Lin, J.-F.: Reconciliation of experiments and theory on
407 transport properties of iron and the geodynamo. Physical review letters
408 **125**(7), 078501 (2020)

409 [14] Zhang, Y., Luo, K., Hou, M., Driscoll, P., Salke, N.P., Minár, J.,
410 Prakapenka, V.B., Greenberg, E., Hemley, R.J., Cohen, R., et al.: Ther-
411 mal conductivity of fe-si alloys and thermal stratification in earth's core.
412 Proceedings of the National Academy of Sciences **119**(1) (2022)

413 [15] Pozzo, M., Davies, C.J., Alfè, D.: Towards reconciling experimental and
414 computational determinations of earth's core thermal conductivity. Earth
415 and Planetary Science Letters **584**, 117466 (2022)

416 [16] Nimmo, F.: Thermal and compositional evolution of the core. Treatise on
417 Geophysics **9**, 201–219 (2015)

418 [17] Davies, C., Greenwood, S.: Thermo-chemical dynamics in Earth's core
419 arising from interactions with the mantle. eartharxiv.org **0**(0), 0 (2022)

420 [18] O'Rourke, J.G., Stevenson, D.J.: Powering Earth's dynamo with magne-
421 sium precipitation from the core. Nature **529**(7586), 387–389 (2016)

422 [19] Badro, J., Siebert, J., Nimmo, F.: An early geodynamo driven by exsolu-
423 tion of mantle components from Earth's core. Nature **536**(7616), 326–328
424 (2016)

425 [20] Badro, J., Aubert, J., Hirose, K., Nomura, R., Blanchard, I., Borensztajn,
426 S., Siebert, J.: Magnesium partitioning between Earth's mantle and core
427 and its potential to drive an early exsolution geodynamo. Geophysical
428 Research Letters **45**(24), 13–240 (2018)

[21] Du, Z., Jackson, C., Bennett, N., Driscoll, P., Deng, J., Lee, K.K., Greenberg, E., Prakapenka, V.B., Fei, Y.: Insufficient energy from MgO exsolution to power early geodynamo. Geophysical Research Letters **44**(22), 11–376 (2017)

[22] Du, Z., Boujibar, A., Driscoll, P., Fei, Y.: Experimental constraints on an mgo exsolution-driven geodynamo. Geophysical Research Letters **46**(13), 7379–7385 (2019)

[23] Hirose, K., Morard, G., Sinmyo, R., Umemoto, K., Hernlund, J., Helffrich, G., Labrosse, S.: Crystallization of silicon dioxide and compositional evolution of the Earth's core. Nature **543**(7643), 99–102 (2017)

[24] Helffrich, G., Hirose, K., Nomura, R.: Thermodynamical modeling of liquid Fe-Si-Mg-O: Molten magnesium silicate release from the core. Geophysical Research Letters **47**(21), 2020–089218 (2020)

[25] Takafuji, N., Hirose, K., Mitome, M., Bando, Y.: Solubilities of o and si in liquid iron in equilibrium with (mg, fe) sio3 perovskite and the light elements in the core. Geophysical Research Letters **32**(6) (2005)

[26] Rubie, D.C., Jacobson, S.A., Morbidelli, A., O'Brien, D.P., Young, E.D., de Vries, J., Nimmo, F., Palme, H., Frost, D.J.: Accretion and differentiation of the terrestrial planets with implications for the compositions of early-formed solar system bodies and accretion of water. Icarus **248**, 89–108 (2015)

[27] Fischer, R.A., Nakajima, Y., Campbell, A.J., Frost, D.J., Harries, D., Langenhorst, F., Miyajima, N., Pollok, K., Rubie, D.C.: High pressure metal–silicate partitioning of Ni, Co, V, Cr, Si, and O. Geochimica et

Cosmochimica Acta **167**, 177–194 (2015)

[28] Mittal, T., Knezek, N., Arveson, S.M., McGuire, C.P., Williams, C.D., Jones, T.D., Li, J.: Precipitation of multiple light elements to power Earth's early dynamo. Earth and Planetary Science Letters **532**, 116030 (2020)

[29] Badro, J., Brodholt, J.P., Piet, H., Siebert, J., Ryerson, F.J.: Core formation and core composition from coupled geochemical and geophysical constraints. Proceedings of the National Academy of Sciences **112**(40), 12310–12314 (2015)

[30] Fischer, R.A., Campbell, A.J., Ciesla, F.J.: Sensitivities of Earth's core and mantle compositions to accretion and differentiation processes. Earth and Planetary Science Letters **458**, 252–262 (2017)

[31] Ma, Z.: Thermodynamic description for concentrated metallic solutions using interaction parameters. Metallurgical and Materials Transactions B **32**(1), 87–103 (2001)

[32] Liu, W., Zhang, Y., Yin, Q.-Z., Zhao, Y., Zhang, Z.: Magnesium partitioning between silicate melt and liquid iron using first-principles molecular dynamics: Implications for the early thermal history of the earth's core. Earth and Planetary Science Letters **531**, 115934 (2020)

[33] Davies, C., Pozzo, M., Gubbins, D., Alfè, D.: Constraints from material properties on the dynamics and evolution of Earth's core. Nature Geoscience **8**(9), 678–685 (2015)

[34] Greenwood, S., Davies, C.J., Mound, J.E.: On the evolution of thermally stratified layers at the top of Earth's core. Physics of the Earth and

Planetary Interiors, 106763 (2021)

[35] Driscoll, P., Bercovici, D.: On the thermal and magnetic histories of Earth and Venus: Influences of melting, radioactivity, and conductivity. Physics of the Earth and Planetary Interiors **236**, 36–51 (2014)

[36] Jaupart, C., Labrosse, S., Lucazeau, F., Mareschal, J.: 7.06-temperatures, heat and energy in the mantle of the earth. Treatise on geophysics **7**, 223–270 (2007)

[37] Abe, Y.: Thermal and chemical evolution of the terrestrial magma ocean. Physics of the Earth and Planetary Interiors **100**(1-4), 27–39 (1997)

[38] Solomatov, V.: Magma oceans and primordial mantle differentiation. In: Schubert, G. (ed.) Treatise on Geophysics vol. 10, pp. 81–104. Elsevier, Amsterdam (2015)

[39] Hohenberg, P., Kohn, W.: Inhomogeneous electron gas. Physical review **136**(3B), 864 (1964)

[40] Kohn, W., Sham, L.J.: Self-consistent equations including exchange and correlation effects. Physical review **140**(4A), 1133 (1965)

[41] Pozzo, M., Davies, C., Gubbins, D., Alfe, D.: FeO content of Earth's liquid core. Physical Review X **9**(4), 041018 (2019)

[42] Kresse, G., Furthmüller, J.: Efficient iterative schemes for ab initio total-energy calculations using a plane-wave basis set. Physical review B **54**(16), 11169 (1996)

[43] Nosé, S.: A unified formulation of the constant temperature molecular dynamics methods. The Journal of chemical physics **81**(1), 511–519

(1984)

[44] Kresse, G., Joubert, D.: From ultrasoft pseudopotentials to the projector augmented-wave method. Physical review b **59**(3), 1758 (1999)

[45] Perdew, J.P., Chevary, J.A., Vosko, S.H., Jackson, K.A., Pederson, M.R., Singh, D.J., Fiolhais, C.: Atoms, molecules, solids, and surfaces: Applications of the generalized gradient approximation for exchange and correlation. Physical review B **46**(11), 6671 (1992)